Emergent Materials (2024) 7:1715–1731
https://doi.org/10.1007/s42247-024-00696-z

ORIGINAL ARTICLE

Luminescence features of Dy^{3+}-doped B_2O_3 and B_2O_3-P_2O_5 hosts for optical devices: the linear and non-linear optical studies

P. Deepa[1] · Priya Murugasen[2] · A. Antony Suresh[2] · M. Dhavamurthy[1] · A. V. Deepa[3]

Received: 6 January 2024 / Accepted: 29 March 2024 / Published online: 24 April 2024

Abstract

The glass with various concentrations of trivalent rare earth Dy^{3+} in borate and boro-phosphate host structures, along with alkali and transition metals, was synthesized by the melt-quenching technique. An FT-IR and FT-Raman spectrum reveal the structural features by tracing out the various molecular vibrations of borate and phosphate units. UV–Vis-NIR spectral analysis was used to investigate the effect of RE concentration on linear (E_g, ΔE, n_1, and $\chi^{(1)}$) and non-linear ($\chi^{(3)}$, n_2) optical characteristics. The metal–oxygen bond character is explored in relation to the impact of alkali cations on the $\chi^{(3)}$ of alkali borate and boro-phosphate host glasses. Photoluminescence emission spectra obtained in the optical zone show two intense band emissions traced at 482 and 574 nm, which correspond to $^4F_{9/2} \rightarrow {}^6H_{15/2}$ (electric-dipole transition) and $^4F_{9/2} \rightarrow {}^6H_{13/2}$ (magnetic-dipole transition), respectively, and one weak emission at 674 nm, which corresponds to $^4F_{9/2} \rightarrow {}^6H_{11/2}$. The fluorescence decay time was measured and fitted with the characteristics of a non-exponential decay profile. The estimated color coordinates are in the white region of the CIE 1931 chromaticity curve and are quite close to the conventional white illuminant (0.330, 0.330). In addition, the computed yellow-to-blue (Y/B) ratio and correlated color temperature of the prepared photonic glasses could allow tweaking white light emission via varying concentrations and host environments, which might be advantageous for various optical-based device fabrications.

Keywords Urbach energy · Non-linear optics · Luminescence decay · I-H fit curve

1 Introduction

To develop laser science and technology, non-linear optical (NLO) active compounds can advantageously widen the few coherent spectrum sources currently available to far larger spectral regions. Despite its exceptional expandability, there is a strong need to investigate innovative NLO compounds with superior efficiency and performance for prospective photonic applications. The phosphate glasses were primarily studied as hosts for laser and optical amplifiers owing to their high gain properties in comparison to other glass families [1]. The structure of borate glasses is especially fascinating due to the boron anomaly, and as a result, the impact of the network modifier and generated non-bridging oxygens on the linear and non-linear optical properties may be segregated. Because of their considerable effect on luminous efficiency, B_2O_3-based glasses are widely recognized for their photo-generated second-order NLO effects.

Borate glasses can generate superstructures of B_2O_3 due to the triangular planer BO_3, and tetrahedral BO_4 may interact to form diborate ($B_2O_5^{4-}$), tetraborate/pyroborate ($B_4O_7^{2-}$), pentaborate (B_5O_8), or boroxol ring, depending on the quantity of non-bridging oxygens (NBOs) or bridging oxygens (BOs). Alkali metals (Li, Na, and K) modify borate glass, and the emergence of different structural units causes a notable alteration in its physical characteristics [2]. Specifically, lithium borate glasses, which are primarily known as solid electrolytes, are the most adaptable glass systems. One can investigate and synthesize novel materials for optical purposes by adding a specified amount of rare earth oxide to these glasses for specific applications. Host materials with low maximal phonon energies are preferred

✉ Priya Murugasen
priyam7373@gmail.com

[1] Department of Physics, Manna Rajagopalaswamy Government Arts College, Tamilnadu 614001, India

[2] Department of Physics, Saveetha Engineering College, Thandalam, Chennai 602 105, India

[3] Department of Physics, Mohammed Ali Shihab Thangal Memorial Arts & Science College, Perinthalmanna, Malappuram 679325, India

to synthesize rare earth ions-doped glasses since rare earth ions consume less excitation energy during non-radiative transitions, which leads to relatively high luminous quantum efficiencies. Typically, the maximal phonon energies of the hosts with oxides, such as boron oxides (B_2O_3) and phosphorous pentoxide (P_2O_5), are higher than those of the hosts with halide and sulfur. However, the study found that the inclusion of alkali and alkaline metal ions in the oxide glasses substantially reduces phonon energy through energy transfer interactions.

Heavy metal oxide-based RE-infused glass networks have large lasing abilities due to their lower field strength and higher mass and polarizability [3]. The doping concentration of Dy^{3+} should be considered because it affects both the optical transition properties of the material and the concentration quenching of fluorescence intensity caused by the cross-relaxation between Dy^{3+} existents. Several researchers reported that concentration quenching occurs at high doping concentrations (≥ 1.0 mol%) of Dy_2O_3 in glasses, so many have studied the glass systems with only 1.0 mol% of Dy2O3 [4–6]. In their ground state, lanthanide ions (Dy^{3+}) have an electronic structure of [Xe] $4f^{10}$ $5S^2$ $5p^6$, where the f-electrons are typically non-bonding since they are protected by the $5S^2$ $5p^6$ orbitals. The optical characteristics are known to be primarily influenced by the configuration and number of 4f electrons. The NLO properties for lanthanide glasses are predicted to be improved because of the optical resonance phenomenon, which is followed by f–f electron transitions. According to reports, the inclusion of TiO2 in glass compositions improves the NLO factors of the glasses due to their empty d-shells and lone pair electrons [7]. The addition of Al_2O_3 in a sample improves the optical sensitivity by changing the host structure and generating asymmetric sites that result in a 30% increase in the PL intensity when compared to non-Al_2O_3 samples [8].

The current paper deals with a study of the Dy^{3+} ion in borate and boro-phosphate host matrixes, together with heavy metal ions. The effects of the Dy^{3+} doping concentration on the transition, quantum effectiveness, quenching state, and luminescence features were studied. Finally, the values of the CIE chromaticity coordinates are assessed to confirm the w-LED application.

2 Experimental technique

Glasses with the chemical compositions of $(60-x)B_2O_3 + 25SrCO_3 + 7TiO_2 + 5LiCO_3 + 3Al_2O_3 + xDy_2O_3$ ($x = 0.10$, 0.25, 0.50, and 1.00 mol%) and $40B_2O_3 + 20SrCO_3 + 20H_6NO_4P + 7ZnO + 5LiCO_3 + (5-x)P_2O_5 + 3Al_2O_3 + xDy_2O_3$ ($x = 0.25$ and 0.50 mol%), respectively, were synthesized by melt quenching technique. The boron oxide (B_2O_3) and phosphorous pentoxide (P_2O_5) act as a network former in the respective glasses; $SrCO_3$ acts as a network modifier; aluminum oxide (Al_2O_3) will increase network connectivity; ZnO will increase the mechanical stability of the glass. The measured quantity of AR-grade chemicals was taken and mixed thoroughly to attain homogeneity in an agate mortar. The blended chemicals were placed in an alumina crucible and heated in an electric furnace for 7 h at 1125 °C. After quickly pouring the melt onto a preheated brass metal plate, the samples were annealed at 400 °C to reduce internal stress and achieve structural stability. For convenience, the borate host glasses are designated as BDy0.10, BDy0.25, BDy0.50, and BDy1.0, and the boro-phosphate host glasses are designated as BPDy0.25- and BPDy0.50-based on the Dy^{3+} concentration.

3 Characterization techniques

3.1 FT-IR spectral analysis

Thin pellets of approximately 3 mm in thickness were made by mixing KBr, and powdered glass samples were subjected to FT-IR measurements. The spectra were taken at room temperature with a JASCO FTIR 6100 spectrometer with a resolution of 0.5 cm^{-1} in the 400–4000 cm^{-1} wavenumber range. The FTIR spectra of borate glass systems are depicted in Fig. 1a. The peak at 702 cm^{-1} confirmed the bending vibration of the B-O-B linkage of the penta-borate unit and the vibration of linking oxygen atoms ($BO\emptyset_2^-$). The presence of B-O bond stretching vibrations of tetrahedral BO_4 units is responsible for the small band at 870 cm^{-1} [9]. The peak at 1020 cm^{-1} is caused by pentaborate as well as BO_4 tetrahedral vibrations [10]. The peaks at 1214 cm^{-1} and 1346 cm^{-1} correspond to B–O asymmetric stretching vibrations in ortho-borate groups and B–O stretching vibrations of BO_3 trigonal units in ortho-, pyro-, and meta-borate units, respectively. A change in the oxygen-to-boron ratio is enhanced by the substitution of B_2O_3 with a significant concentration of metal oxides such as TiO_3 and $Al2O_3$, along with an increase in Dy_2O_3 concentrations, resulting in stable BO_4 units. The creation of BO_4 units results in tightly packed glass structures, and it decreases the absorption intensity [11]. It was determined that there were no –OH molecules present in the BDy0.10, BDy0.25, and BDy1.0 glasses because this IR band of these materials did not explore the peak associated with the OH vibration position. In BDy0.5 glass, there are two distinct small-intense peaks at 2852 and 2928 cm^{-1} showing the presence of a smaller quantity of OH molecules. The weakened OH content indicates improved quantum efficiency and lower non-radiative losses for the RE-doped luminous materials [12]. The presence of water

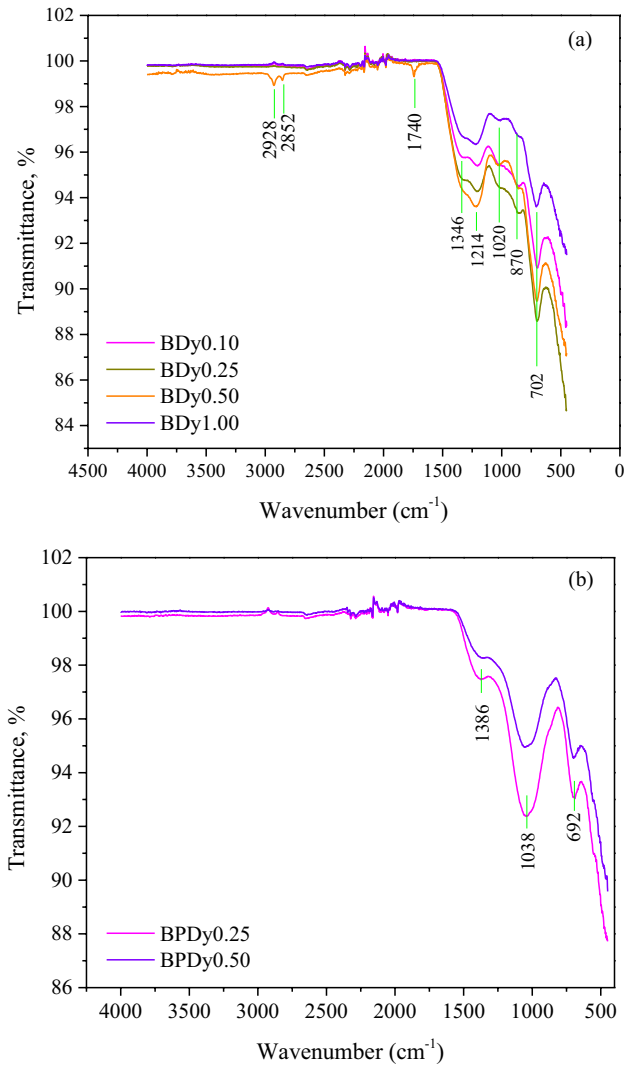

Fig. 1 FT-IR spectral analysis of (**a**) BDy_x ($x = 0.10$, 0.25, 0.50, and 1.00 mol%) and (**b**) $BPDy_x$ ($x = 0.25$ and 0.50 mol%)

molecules or hydroxyl-related bands is further validated by the significant peak that occurred at 1740 cm^{-1} in BDy0.5 glass.

Figure 1b demonstrates the vibrational spectrum of BPDy0.25 and BPDy0.50 glass systems. The peak at 692 cm^{-1} is instigated by P–O–P bending vibrations, and the band at 1038 cm^{-1} is formed by the symmetric stretching vibrations of the B–O–P bridge between borate (BO_4) and phosphate (PO_4) units, as well as the B–O stretching in BO_4 tetrahedra [13]. The well-defined small band at 1386 cm^{-1} dominates the infrared spectrum of boro-phosphate glass matrix in the 800 to 1600 cm^{-1} spectral range as the predominant contribution of Q^2 ($[P(OP)_2(O^-)_2]$) and BO_3 units. The minor peaks traced between 2000 and 2500 cm^{-1} confirm the presence of a hydroxyl group.

3.2 Raman spectral analysis

The FT-Raman spectra were taken with a Bruker RFS 27 Multi-RAM spectrometer with a resolution of 2 cm^{-1}. Because of their intriguing properties, such as the boron anomalies, B_2O_3-based glasses have received a lot of attention over the years. The Raman spectrum of BDy0.5 glass reveals a significant number of bands caused by the vibration of BO_4 and BO_3 groups, as well as complexes including $[BO_3]^{3-}$ and $[BO_4]^{5-}$ groups. The spectrum, as shown in Fig. 2a, reveals a significant intensity band at 102 cm^{-1}, which is associated with the symmetric stretching vibration of heavy metal ions, such as Sr–O and Ti–O bonds. The small-broaden peak at 459 cm^{-1} is ascribed to B–O–B ring angle bending, which is seen at 470 cm^{-1} for pure B_2O_3. The asymmetric structure of a highly intense peak centered at ~ 852 cm^{-1} is caused by B–O–B symmetric stretching in pyro-borate units [14]. Three peaks were detected through band deconvolution at 709, 794, and 870 cm^{-1}, respectively. The modest intensity band at 709 cm^{-1} is accredited to the γ-vibration of $[BO_3]^{3-}$/symmetric breathing vibration of boroxol rings with two BO_4 groups. The presence of a six-membered boron (boroxol) ring [15] in the prepared glass is indicated by the Raman band nearly observed at 800 cm^{-1} (in our case 794 cm^{-1}). The 794 and 870 cm^{-1} peaks were due to symmetric breathing vibrations of the boroxol ring containing one BO_x unit (penta-, tetra-, or tri borate), and the symmetric stretching of $[BO_3]^{3-}$ units, respectively [16, 17]. Peaks at 993 and 1281 cm^{-1} indicate that the borate host glass contains $B–O^-$ symmetric stretching vibrations in penta-borate ($B_5O_8^-$) and pyro-borate ($B_3O_5^{4-}$) anionic groups, respectively [14, 18].

The first band edge in the region of 1200–1450 cm^{-1}, specifically at 1208 cm^{-1}, is accountable for the asymmetric stretching vibration of $[BO_3]^{3-}$ units. The band shoulder at 1353 cm^{-1} is associated with the $BØ_2O^-$ triangles linked to $BØ_4^-$ units (O^-: non-bridging oxygen atom, and Ø: bridging oxygen atom between the two boron atoms) [19]. The peak at 1421 cm^{-1} is due to the B–O stretching vibrations of the meta-borate (BO_2^-) chains and rings. The bands in the Raman spectra of BDy0.5 glass may have widened due to the anharmonicity of the interaction between the BO_4 groups in the borate rings and the Li-ions. A strong network structure is created because the emergence of BO_4 units in the case of lithium ions is greatly influenced by the mass of the alkali ion [20]. The emergence of a peak after 1900 cm^{-1} may be due to the presence of hydroxyl group vibration in the glass system.

The Raman spectrum of BPDy0.5 is depicted in Fig. 2b, and when P_2O_5 is replaced with B_2O_3, the structural network of this glass exhibits consequently significant modifications. A significant intense peak detected in the lower wavenumber region at ~ 91 cm^{-1} reveals the vibration of heavy metal ions

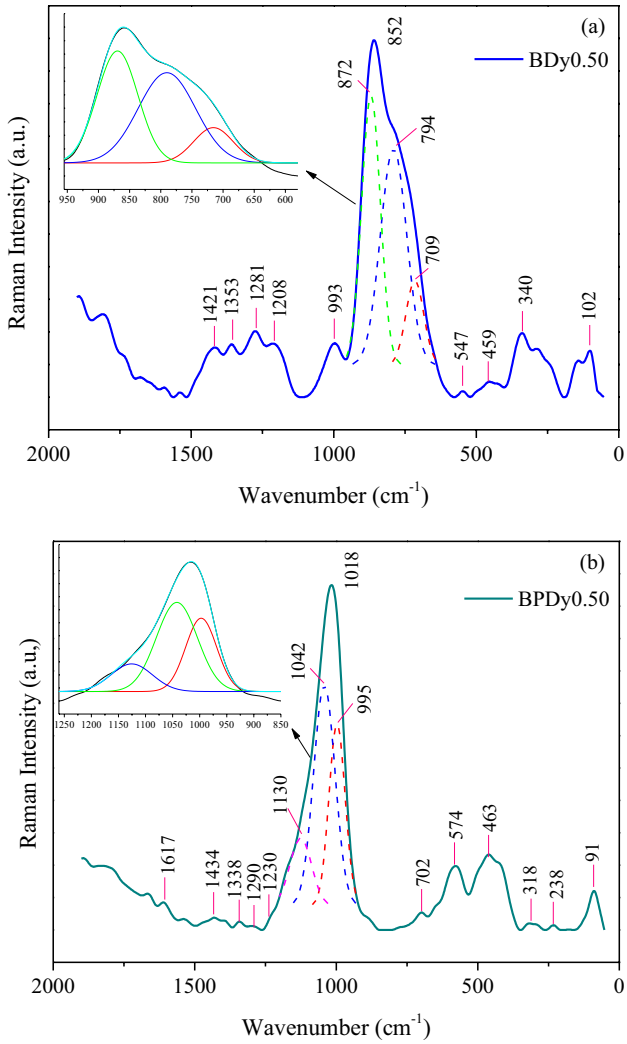

Fig. 2 FT-Raman spectral analysis of (**a**) BDy0.50 and (**b**) BPDy0.50

with the binding oxygen, and it was observed nearly identical location in BDy0.5 glass. The weak vibrations brought on by PO_2 bending and bending motions in O–P–O linkages are discernible at 238 and 318 cm^{-1}, respectively [21]. The broad band with a sharp edge at 463 cm^{-1} and the consecutive band at 574 cm^{-1} were attributed to the independent di-borate group vibrations, and O–P–O bending vibrations of PO_4^{3-} tetrahedral units [22, 23]. The band at 713 cm^{-1} originates from the P–O–P symmetric stretching vibrations, which are produced by the binding oxygen atoms connecting the neighboring PO_4 tetrahedral units. The strong and intense peak at 1018 cm^{-1} is responsible for the P–O symmetric stretching vibration of the Q^1 terminal group. The observed band with a center at 1018 cm^{-1} is asymmetric, and the bulge in the higher wavenumber zone is caused by the overlap of the ~ 1130 cm^{-1} and ~ 1230 cm^{-1} bands, which are the locations of the symmetric and asymmetric stretching of non-binding (PO_2) of Q^2 units, respectively [24]. The deconvoluted peak at 995 cm^{-1} within a large band is designated to the orthophosphate (PO_4^{3-}) group symmetric stretching vibration of the Q^0 units [23]. The detectable band at 1290 cm^{-1} may be associated with the combined vibration of boro-phosphate groups [24]. The moderate peak identified at 1338 cm^{-1} is caused by the P = O stretching vibration of terminal oxygen. The tiny-band edge detected at 1434 cm^{-1} is revealed for the stretching vibration of molecular oxygen bands and B–O in non-bridging oxygen of $[BO_3]^{3-}$ triangles. The peak emergence in the higher region around 1600 cm^{-1} is ascribed to the OH-bending vibration. Tables 1 and 2 show a description of the vibrational bands found in the FT-IR and FT-Raman spectra of the prepared glasses.

3.3 UV–Vis spectral analysis: optical characterization

Optical absorption spectra of the BDy_x ($x = 0.10$, 0.25, 0.50, and 1.00 mol%) and $BPDy_x$ ($x = 0.25$ and 0.50 mol%) glasses were performed in the JASCO V-670 spectrometer at a wavelength between 190 and 1400 nm at room temperature. Figure 3a and b depicts the collected spectra of the Dy^{3+}-doped borate and boro-phosphate host glasses, respectively. The optical absorption spectra of Dy^{3+}-doped glasses are divided into two sets of manifolds in the UV–Vis (350–550 nm) and near-infrared (715–2000 nm) ranges [25]. The comparatively strong spin-allowed transitions that dominate the near-infrared region of the spectrum are its defining feature. Four absorption bands are originating from the ground state ($^6H_{11/2}$) of the Dy^{3+} traced out in the intermediate spectral region of both the glass matrixes. The absence of bands in a lower wavelength region (UV–Vis) is caused by the strong absorption of the hosts via the closed packing of heavy metal ions. In addition, it was observed that the absorption peak intensity increased and resolved their positions while increasing the Dy^{3+} ion concentration in the glass matrices. The four observed dominant absorption band locations and their excited states are as follows: 801 nm ($^6F_{5/2}$), 900 nm ($^6F_{7/2}$), 1086 nm ($^6F_{9/2}$), and 1262 nm ($^6F_{11/2}$). The positions of the absorption bands in the two host glasses are nearly identical. The ligand environment has an impact on the location and intensities of several transitions of Dy^{3+} ions. The transition $^6H_{11/2} \rightarrow {}^6F_{11/2}$ has a relatively high intensity compared to the others, and it is termed to be a hypersensitive transition that obeys the selection rules $\Delta L \leq 2$, $\Delta \leq 2$, and $\Delta S = 0$. The visible region's bands are spin-prohibited and have a weak cross-section, at least up to 400 nm, and thus pose a serious obstacle to the emergence of effective visible laser media.

The optical band gap energies are calculated using the diffused reflectance data of BDy_x and $BPDy_x$ glasses in the Kubelka–Munk (K-M) theory [26]. The K-M function F(R) in this case is related to the absorption coefficient (α),

Table 1 FT-IR and FT-Raman spectroscopic vibrational assignments for the BDy0.5 glass (borate host)

Wavenumber (cm^{-1})		Vibrational assignments
FT-IR	FT-Raman	
–	102	Symmetric stretching vibration of heavy metal ions including Sr–O and Ti–O bonds
702	–	Bending vibration of the B–O–B
–	709	γ-vibration of $[BO_3]^{3-}$/symmetric breathing vibration of boroxol rings with two BO_4 groups
–	794	Symmetric breathing vibrations of boroxol ring containing one BO_4 units (penta-, tetra-, or triborate) and the symmetric stretching of $[BO_3]^{3-}$ units
–	852	B–O–B symmetric stretching in pyroborate units
870	870	B–O bond stretching vibrations of tetrahedral BO_4 units and symmetric stretching of $[BO_3]^{3-}$ units
–	993	$B–O^-$ symmetric stretching vibrations in pentaborate ($B_5O_8^-$) and pyro-borate ($B_3O_5^{4-}$) anionic groups
1020	–	Pentaborate along with the BO_4 tetrahedral stretching vibrations
–	1208	Asymmetric stretching vibration of $[BO_3]^{3-}$ units
1214	–	B–O asymmetric stretching vibration in orthoborate group
–	1281	$B–O^-$ symmetric stretching vibrations in pyroborate ($B_3O_5^{4-}$) anionic groups
1346	–	B–O stretching vibrations of BO_3 trigonal units in ortho-, pyro-, and meta-borate units
–	1353	Stretching vibrations of $BØ_2O^-$ triangles linked to $BØ_4^-$ units
–	1421	B–O stretching vibrations of the meta-borate (BO_2^-) chains and rings
1740	–	Bending vibrations of the hydroxyl group
2852, 2928	–	Stretching vibration of –OH molecules

Table 2 FT-IR and FT-Raman spectroscopic vibrational assignments for the BPDy0.5 glass (boro-phosphate host)

Wavenumber (cm^{-1})		Vibrational assignments
FT-IR	FT-Raman	
–	91	Vibration of heavy metal ions including Sr–O and Ti–O bonds
–	238	PO_2 bending vibration
–	318	Bending motions in O–P–O linkages
–	463	Independent di-borate groups vibrations,
–	574	O–P–O bending vibrations of PO_4^{3-} tetrahedral units
692	–	P–O–P bending vibrations
–	713	P–O–P symmetric stretching vibrations
–	995	Orthophosphate (PO_4^{3-}) group symmetric stretching vibration of the Q^0 units
–	1018	P–O symmetric stretching vibration of Q^1 terminal group
1038	–	Combined vibrations about the symmetric stretching of B–O–P bridge between BO_4 and PO_4 units and B–O stretching vibrations in BO_4 tetrahedra
–	1130, 1230	Symmetric and asymmetric stretching of non-binding (PO_2) of Q^2 units
–	1290	Combined vibration of borate and phosphate groups
	1338	P = O stretching vibration of terminal oxygen
1386	–	Stretching vibrations of Q^2 ($[P(OP)_2(O^-)_2]$) and BO_3 units
–	1434	Stretching vibration of molecular oxygen bands and B–O in non-binding oxygen of $[BO_3]^{3-}$ triangles
–	1617	OH^- bending vibration
2000–2500	–	hydrogen bonding in B–OH and P–OH units caused by the presence of hydroxyl group

diffusion coefficient (S), and reflectance (R) of an infinitely thick layer, as given below:

$$F(R) = \frac{\alpha}{S} = \frac{(1-R)^2}{2R} \quad (1)$$

$$F(R)\, h\upsilon = B\left(h\upsilon - E_g\right)^{\gamma} \quad (2)$$

Here, the values of $\gamma = 2$ and ½ for indirect and direct transitions are measured by extrapolating the linear sections of the curve to intersect the hυ axis at $(F(R)h\upsilon)^{1/2} = 0$ and $(F(R)h\upsilon)^2 = 0$, respectively, as shown in Figs. 4 and

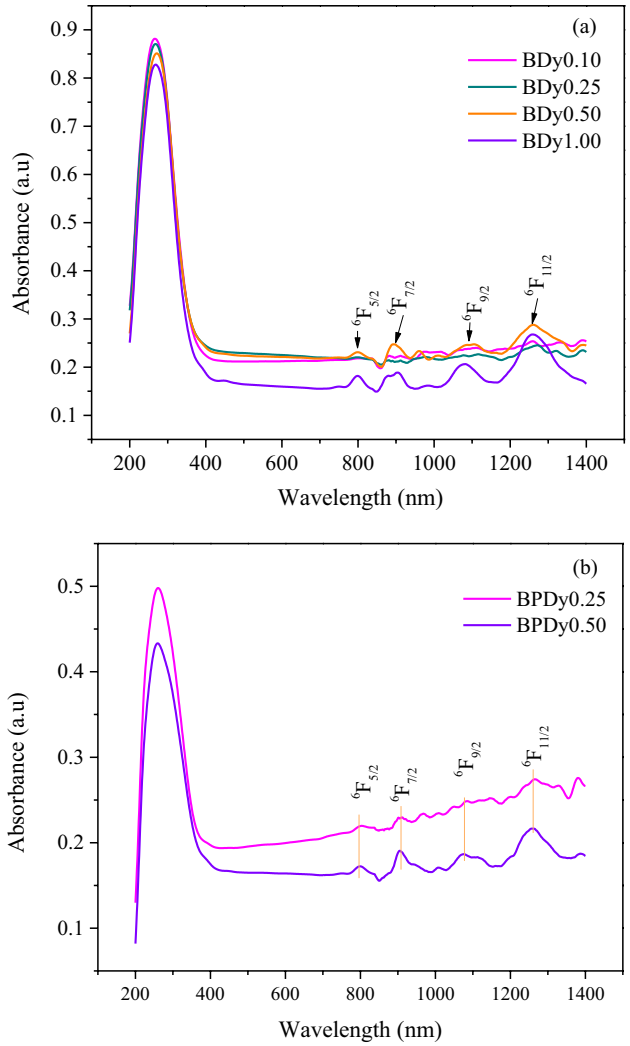

Fig. 3 UV–Vis spectral analysis: optical absorption of (**a**) BDy_x ($x=0.10$, 0.25, 0.50, and 1.00 mol%) and (**b**) $BPDy_x$ ($x=0.25$ and 0.50 mol%)

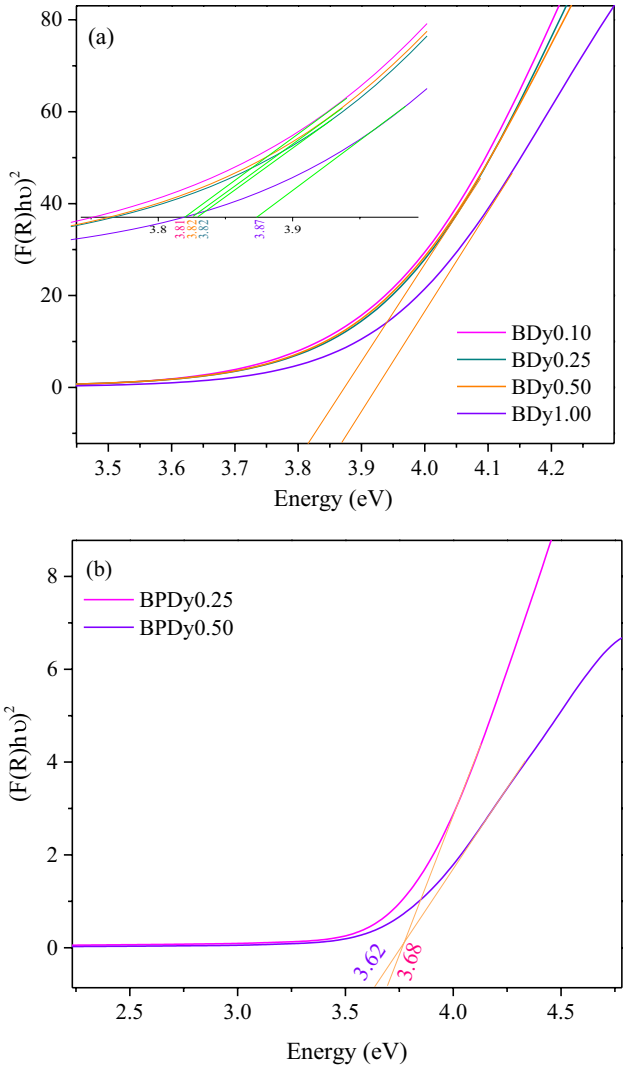

Fig. 4 Kubelka–Munk plot: direct band-gap energy of (**a**) BDy_x ($x=0.10$, 0.25, 0.50, and 1.00 mol%) and (**b**) $BPDy_x$ ($x=0.25$ and 0.50 mol%)

5. The calculated values of direct and indirect band gap energy of the glasses vary from 3.81 to 3.87 eV and 2.73 to 3.33 eV, respectively, with an increase in Dy^{3+} concentration in borate host matrixes (BDy_x), as shown in Figs. 4a and 5a. At initial, the band gap was low as Dy_2O_3 generated non-bridging oxygens in the borate host matrix; the optical band gap was increased with the further addition of Dy_2O_3, which was formed by the substitution of boron ions (0.85 Å) with greater atomic radii (0.91 Å) Dy^{3+} ions. The optical characteristics of the glasses changed when Dy^{3+} ions were added to the lattice owing to more energy levels being generated within the band gap. In the borate glass matrix, the band gap energy increases with the Dy^{3+} ion concentration (Table 3) by contributing additional conduction electrons, which then occupy the conduction band at energies greater than the conduction band minimum. As a result, the larger energy differences between conduction and valence bands also influenced the absorption and emission. The energy difference between these bands in an indirect band gap material also includes the change of electron momentum, which is associated with the presence of phonon.

This behavior change could be associated with structural changes in the matrix that modify binding strength. However, as the concentrations of Dy^{3+} in the boro-phosphate host matrixes increase, the band gap energies decrease from 3.68 to 3.62 eV (direct band gap) and 2.82 to 2.75 eV (indirect band gap), as shown in Figs. 4b and 5b. According to Safeya et al., the rate of conversion of $[BO_3] \rightarrow [BO_4]$ increases the inclusion of modifier oxides into the borate host structure [27]. Whereas in the phosphate host, the inclusion of modifier oxides results in the high formation of

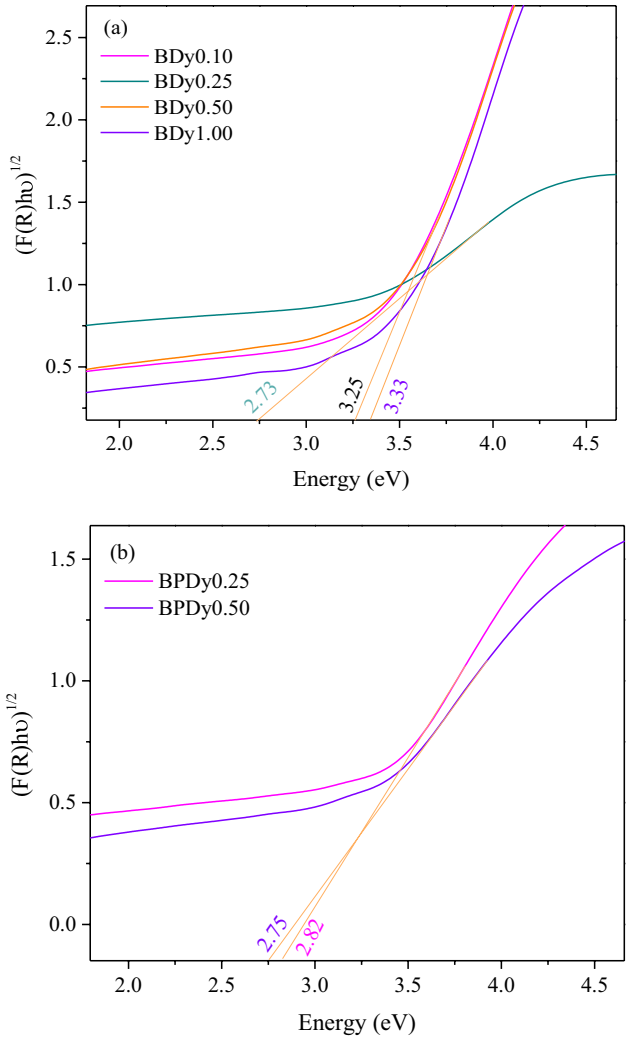

Fig. 5 Kubelka–Munk plot: indirect band-gap energy of (**a**) BDy_x (x=0.10, 0.25, 0.50, and 1.00 mol%) and (**b**) $BPDy_x$ (x=0.25 and 0.50 mol%)

negative non-bridging oxygen, which is balanced with the positive cations.

In an amorphous structure, the absorption edge indicates the presence of inter-band transition tails, and Urbach energy (ΔE) is a crucial factor that determines the level of disordering in the networks; it was calculated using the relation:

$$\alpha\ (\upsilon\ ) = \alpha\ _{o}\ exp\ (h\upsilon\ /\Delta E) \tag{3}$$

The quantity of ΔE signifies the width of localized states, including vacancies, defects due to concentrations, and dangling bonds. As a result, determining the Urbach energy and characterizing the degree of material imperfection are made possible by analyzing the optical absorption spectrum region corresponding to the density of state tails. The Urbach energy measures the steepness of the absorption beginning close to the band edge and, in consequence, the width of the density states. The Urbach energy (ΔE) values (~0.80 eV) were measured from the slope of the linear section of both the glass matrixes and are displayed in Fig. 6a and b. Table 3 displays the measured Urbach's energy values of both BDy_x and $BPDy_x$ glass matrixes. The measured ΔE value decreases in borate host glasses, whereas its value increases in boro-phosphate glasses with an increase in Dy^{3+} ion concentrations. The low value of ΔE values suggested that the prepared borate host structures have a relatively high organized structure, and it is indicated by a stronger absorption onset. Since h energy and the band gap energy E_g have an inverse relationship, a sample with a larger band gap is anticipated to have a smaller band tail. Furthermore, the lower Urbach energy of the borate-host glasses implies a reduced disorder of phonon states, hence enhancing the emission features including its purity. The increase in ΔE values in $BPDy_x$ glasses is due to the increased quantity of non-bridging oxygens and is ascribed to the short-range order of their structure.

The linear refractive index (n) was calculated from the indirect optical band gap energy (E_g) of the glasses using:

Table 3 Linear (E_g, n_1) and non-linear optical ($\chi^{(1)}$, $\chi^{(3)}$, and n_2) characteristics of BDy_x (x=0.10, 0.25, 0.50, and 1.00) and $BPDy_x$ (x=0.25 and 0.50)

Glass	$E_{g\text{-dir}}$ (eV)	$E_{g\text{-indir}}$ (eV)	ΔE (eV)	n_1	TPA (cm/GW)	$\chi^{(1)}$ esu	$\chi^{(3)}\times10^{-12}$ esu	$n_2\times10^{-11}$
Dy doped in borate host								
BDy0.10	3.81	3.25	0.801	2.332	10.435	0.3533	2.6509	4.2821
BDy0.25	3.82	2.73	0.809	2.473	14.645	0.4073	4.6786	7.1286
BDy0.50	3.82	3.25	0.821	2.332	10.435	0.3533	2.6509	4.2821
BDy1.00	3.87	3.33	0.746	2.365	9.787	0.3657	3.0406	3.4047
Dy doped in boro-phosphate host								
BPDy0.25	3.68	2.82	1.344	2.447	13.918	0.3971	4.2279	6.5103
BPDy0.50	3.62	2.75	1.519	2.467	14.485	0.4049	4.5711	6.9818
DFBP [53]	2.88	2.69	0.418	2.48				

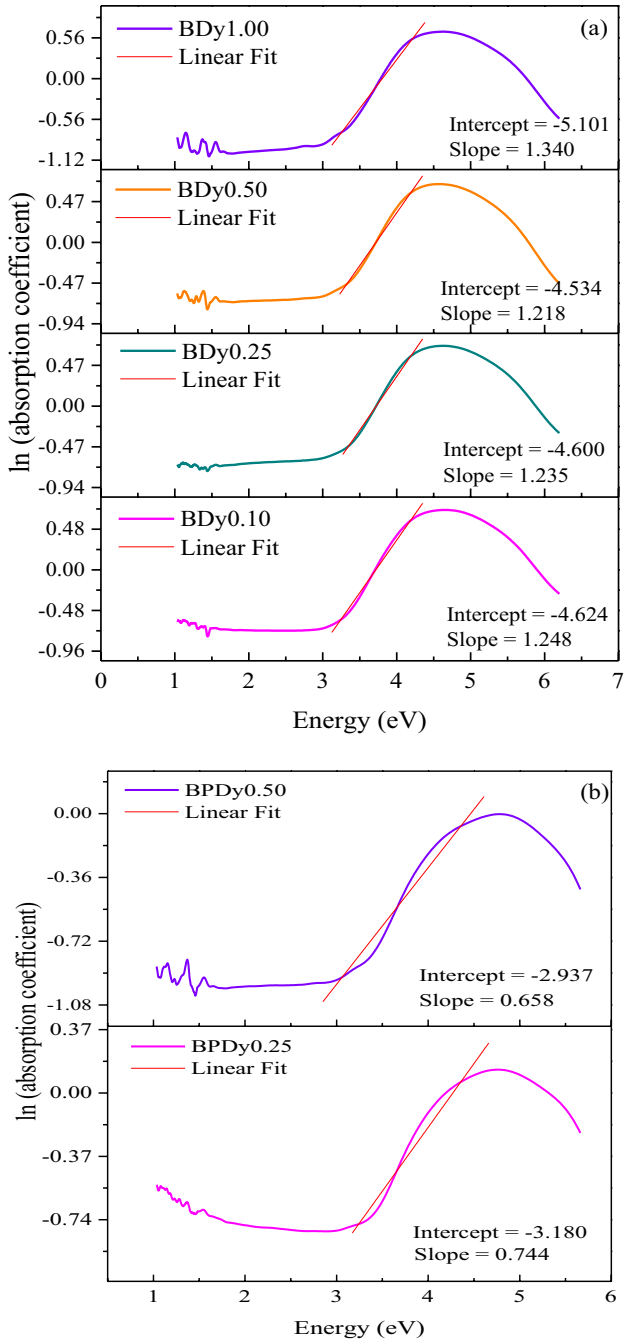

Fig. 6 Urbach energy of (**a**) BDy_x (x=0.10, 0.25, 0.50, and 1.00 mol%) and (**b**) $BPDy_x$ (x=0.25 and 0.50 mol%)

$$\frac{n^2-1}{n^2+2}=1-\sqrt{\frac{E_g}{20}} \tag{4}$$

The refractive index dispersion of BDy_x and $BPDy_x$ glasses is shown in Table 3. It is noticeable that increasing the concentration of Dy^{3+} ions increased the refractive index. According to Wemple, materials with a covalent nature display high microscopic oscillator strength due to the substantial band-broadening of the orbitals of molecules, which results in a high refractive index [28]. Therefore, BDy0.25 and BPDy0.50 in borate and borophosphate host matrixes have a high refractive index compared to other prepared glasses in their hosts. Fanderlik [29] reported that the refractive index of the glass is directly related to the glass density, and the glass containing Al_2O_3 has a comparatively large ion size as well as acting as a glass modifier and not a glass former in the studied glasses. The presence of Al^{3+}, Zn^{2+}, Ti^{2+}, and Sr^{3+} ions is responsible for the greater levels of density and electronic polarizability shown in these glass systems. For the boro-phosphate (B_2O_3-P_2O_5) host glasses with free –OH groups, a higher index of refraction and more non-bridging oxygen generation lead to a denser structure. Many authors discovered that the system containing Li_2CO_3 exhibits the highest degree of refraction. Because the refractive index is affected not only by polarizability but also by the molar volume M/ρ, and as a result, a dense structure is predicted as the molar volume decreases [30, 31]. The high refractive index of transition metal-containing glasses including Sr_2O_3 and Ti_2O may be due to these ions' ability to reduce the average oxygen coordination number. This causes the structure to become more compact, which is then reflected in the rise in refractive index.

The two-phonon absorption (TPA) coefficient is an important metric that may be determined by employing indirect optical band gap energy values, and it was used to evaluate the optical switching performance in waveguides [32].

$$TPA = 36.76 - 8.1E_g\ (cm/GW) \tag{5}$$

TPA coefficient of composition BDy1.0 glass is low (9.787 cm/GW), implying their application in waveguides, and measured TPA values (presented in Table 3) demonstrate that TPA may be modified by influencing the optical band gap [33].

3.4 Non-linear optical characterization

Non-linear optical features are caused by non-linear electric polarization, which can be described as follows:

$$P = \chi^{(1)}E + \chi^{(2)}E^2 + \chi^{(3)}E^3 + \ldots \tag{6}$$

where P represents the electric polarization, and χ represents optical susceptibility. In a glass structure with inversion symmetry, $\chi^{(1)}$ is theoretically zero. As a result, the non-linear optical response in glass is dominated by $\chi^{(3)}$. The addition of RE ions to the glass matrix affords them a non-linear optical characteristic. The following equation relates first-order linear optical susceptibility $\chi^{(1)}$ and third-order

non-linear optical susceptibilities $\chi^{(3)}$ and linear refractive indices (n_1) and non-linear refractive indices (n_2) [34]:

$$\chi^{(1)} = \frac{n_1^2 - 1}{4\pi} \tag{7}$$

$$\chi^{(3)} \cong \mathrm{Re}\ \chi^{(3)} = \left[\chi^{(1)}\right]^4 \times 1.7 \times 10^{-10} esu \tag{8}$$

$$n_2 = \frac{12\pi \mathrm{Re}\ \chi^{(3)}}{n_1} \tag{9}$$

Figure 5b depicts the variation of $\chi^{(3)}$ and n_2 with the various concentrations of Dy^{3+} ions in the BDyx glasses. Miller's rule states that the greater the refractive index, the greater the value of $\chi^{(3)}$ [35]. As a result, the high $\chi^{(3)}$ in BDy0.25 from the borate host and BPDy0.50 from the boro-phosphate is caused by the covalent nature of the metal–oxygen bond. The non-linear behavioral patterns of the curves suggested that the concentration of Dy^{3+} influenced the non-linear optical characteristics of prepared glass systems. Alkali cations can influence the total $\chi^{(3)}$ value in alkali borate and boro-phosphate glasses because $\chi^{(3)}$ for pure B_2O_3 glass is quite small ($=2.88\times10^{-14}$ esu) [36], as shown in Table 3. Adir et al. expected that the glasses containing ions with high polarizability would exhibit a substantial $\chi^{(3)}$ value. The fact that the value of $\chi^{(3)}$ steadily rises as E_g falls suggests that E_g is the key factor of the $\chi^{(3)}$ value of all the glasses in the present work. Due to the reduced band gap, there can be an impact caused by optical resonance enhancement. Dysprosium-doped boro-phosphate glasses exhibit higher optical non-linearity than borate glasses due to one-photon absorption [37]. The combined contribution of the Dy^{3+} ion and heavy-metal oxide ions (Ti^{2+} and Sr^{3+}) with high polarizability could further increase $\chi^{(3)}$.

The two types of resonance effects that rise in $\chi^{(3)}$ value are the pre-resonance effect and the rigorous-resonance effect. The rigorous resonance effect termed as $\chi^{(3)}$ values is enhanced dramatically due to the large transition moment to the first excited state. According to Nasu et al. [38], the field strength of rare-earth cations has a significant impact on the non-linearity. The large optical non-linearity is caused by the small field strength ions' inability to bind valence electrons as tightly. The optical band gap value for these glasses is substantially higher than the energy of a photon in the third harmonic beam ($E=1.96$ eV). As a result, the pre-resonance effect can be the primary factor in increasing the $\chi^{(3)}$ in both the host glasses. Table 3 illustrates the linear and non-linear optical parameters of BDy_x ($x=0.10$, 0.25, 0.50, and 1.00) and $BPDy_x$ ($x=0.25$ and 0.50) glasses. The calculated non-linear refractive index (n_2) value of $BDy_{0.25}$. $BPDy_{0.25}$ and $BPDy_{0.50}$ glasses were found to be higher than the other prepared glasses which suggests that these glasses can be utilized in light-regulated optical devices.

3.5 Photoluminescence

The excitation spectra of all the samples were monitored for the emission wavelength of 574 nm. The spectra reveal three predominant peaks at 350, 367, and 388 nm and other minor peaks at 327, 340, 427, 454, and 475 nm, which correspond to transitions of Dy^{3+} ions from the $^6H_{15/2}$ state to the $^4M_{15/2}+{}^6P_{7/2}$, $^4I_{11/2}$, $^4I_{13/2}+{}^4F_{7/2}$, $^6P_{3/2}$, $(^4F,{}^4D)_{5/2}$, $^4G_{11/2}$, $^4I_{15/2}$, and $^6F_{9/2}$ states, respectively, as shown in Fig. 7. The emission spectra were recorded in the 400–700 nm range for the excitation wavelength of 388 nm and are shown in Fig. 8. There are a large number of f-block energy states in Dy^{3+} with $^4F_9$ meta-stable configuration. The luminescent spectrum reveals two strong emission bands at 482 nm due to magnetic-dipole (MD) transition $^4F_{9/2}\rightarrow{}^6H_{15/2}$ (blue), and 574 nm corresponds to the electric-dipole (ED) transition $^4F_{9/2}\rightarrow{}^6H_{13/2}$ (yellow) strongly influenced by the surrounding environment. The emission at 662 nm is attributed to $^4F_{9/2}\rightarrow{}^6H_{11/2}$ (red) transitions and is found to be relatively weak. It was discovered that the emission intensity of the ED transition is greater than the MD transition for the present glasses, and it follows the selection rules $\Delta L=\pm2$ and $\Delta j=\pm2$. However, in comparison to the other two identified emission bands, the emission band in the 662 nm has a low intensity. Among those observed, the $^4F_{9/2}\rightarrow{}^6H_{13/2}$ transition is hypersensitive, and the ligand field surrounding the Dy^{3+} ion site has a significant impact on its strength. Typically, the host has a minute influence on the intensity of the hypersensitive transition, or it changes only slightly from host to host, whereas the intensity of the magnetic-dipole

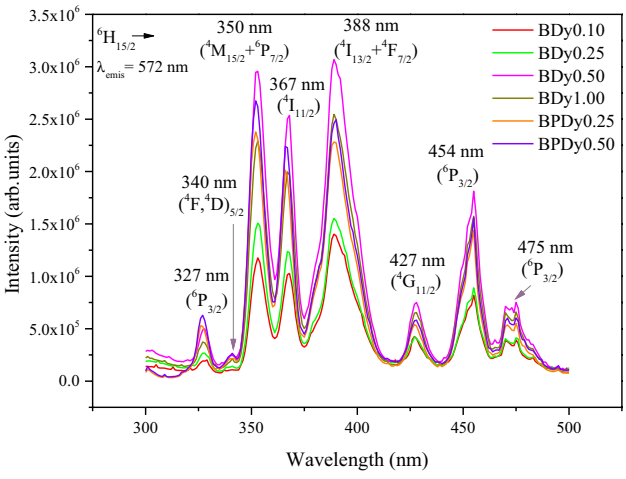

Fig. 7 Photo-excitation spectra of BDy_x ($x=0.10$, 0.25, 0.50, and 1.00 mol%) and $BPDy_x$ ($x=0.25$ and 0.50 mol%)

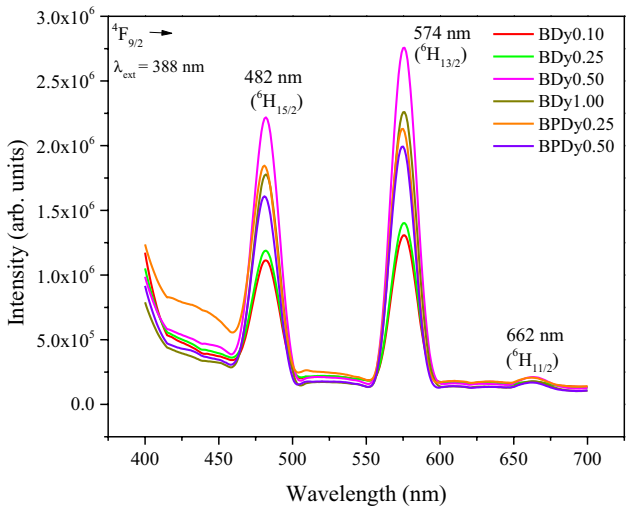

Fig. 8 Photoluminescence spectra of BDy_x ($x = 0.10$, 0.25, 0.50, and 1.00 mol%) and $BPDy_x$ ($x = 0.25$ and 0.50 mol%)

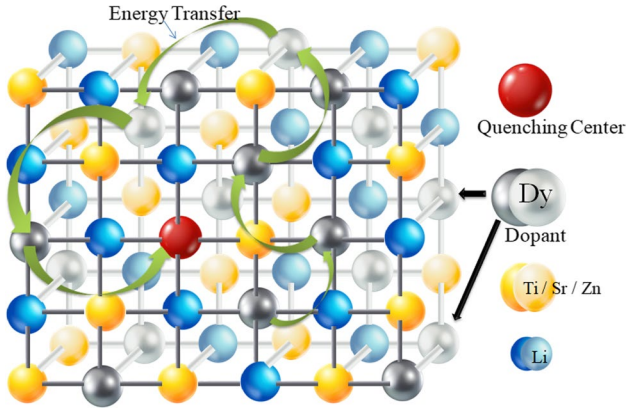

Fig. 9 Schematic representation of concentration quenching mechanism of Dy^{3+}-doped glass matrix

transition varies significantly from host to host [39]. Additionally, the emission of white light has a greater influence on the intensity variation between transitions. The color of the luminescence is nearly white, if the emission intensities of the two transitions ($^4F_{9/2} \rightarrow {}^6H_{15/2}$, $^6H_{13/2}$) are identical, for instance, in the systems $Ba_3Bi(PO_4)^3$:Dy^{3+}, BaY_2ZnO_5:Dy^{3+}, and $(Gd0.98Dy0.02)(BO_2)_3$ [40, 41].

In borate glass system, the intensity of luminescence emission is directly related to their indirect band gap energy. The prepared glasses containing 0.5 and 1 mol% of Dy^{3+} ion concentration have a relatively large band gap. These samples absorb large quantities of high-energy photons, which cause the high-intensity emission. The wider energy gap below the $^4G_{5/2}$ state of Dy^{3+} ion-doped glass substantially reduces the multi-phonon transition rate, even in glass with high-phonon energy. Moreover, the elevated energy states of Dy^{3+} ions impact three emission bands, leading to emission within the visible region.

From Fig. 8, it can be observed that the luminescence intensity rises as the Dy^{3+} ion concentration rises to 0.5 wt% and 0.25 wt% in borate and boro-phosphate host glasses, respectively. As the concentration of Dy^{3+} ions increases in the glass network, the inter-ionic distance decreases gradually, and the exchange interaction among the Dy^{3+} ions becomes robust. When the inter-ionic distance of Dy^{3+}-Dy^{3+} ions is smaller than the critical distance, the tunneling effect is easily activated, leading to cascade energy transfer and luminescence quenching [42]. Figure 9 illustrates the schematic representation of the concentration quenching mechanism in Dy^{3+}-doped host glasses.

Z. Zhu et al. reported that a multi-polar interaction plays an essential role in the concentration quenching mechanism of Dy^{3+} [43]. According to Van Uitert's report, the relationship between activator ion concentration and their emission intensity can be represented as follows [44]:

$$I/x = k\left(1 + \beta(x)^{\theta/3}\right)^{-1} \quad (10)$$

where x = concentration of activator ion; I = intensity of emission; k and β are constant for a given host network under the identical excitation condition; and $\theta = 6$, 8, and 10 values correspond to the different multi-polar interactions. Considering that $\beta(x)\theta/3 >> 1$, then Eq. (10) can be rewritten as:

$$Log(I/x) = \mathrm{K}' - (\theta/3)\,\log(x) \text{ and } K' = \log k - \log \beta \quad (10)$$

The relation between log (x) and log (I/x) and the accompanying straight line has a slope that signifies $-\theta/3$, as shown in Fig. 10a and b for BDy_x and $BPDy_x$ glass, respectively. Herein, the computed average value (both the emission) of $\theta/3$ is 0.718, and θ can be measured as 2.155 for BDy_x glass, whereas the value is 1.150, and θ can be measured as 3451 for $BPDy_x$ glass. The θ value for both glass matrixes was found to be less than 6. The finding indicates that the dipole–dipole (D-D) interaction influences the concentration quenching mechanism of Dy^{3+} emission in borate and boro-phosphate hosts [43, 45]. Table 4 specifies the magnitude of $-\theta/3$ for the individual emission bands of both host glasses.

3.6 Y/A ratio and decay profile

The dominance of yellow emission is the result of a hypersensitive transition, which specifies that the Dy^{3+} ions are positioned at low-symmetry sites without an inversion center. The Y/B value is proportional to the Dy^{3+} concentrations, and it is found to be 1.233–1.352 and 1.218–1.298 for the BDy_x ($x = 0.10$, 0.25, 0.50, and 1.00) and $BPDy_x$ ($x = 0.25$ and 0.50) glasses, respectively. According to Arunkumar et al. [46], a rise in the covalency between Dy^{3+}–O^{2-} ions and the atoms surrounding them in the glasses matrix is

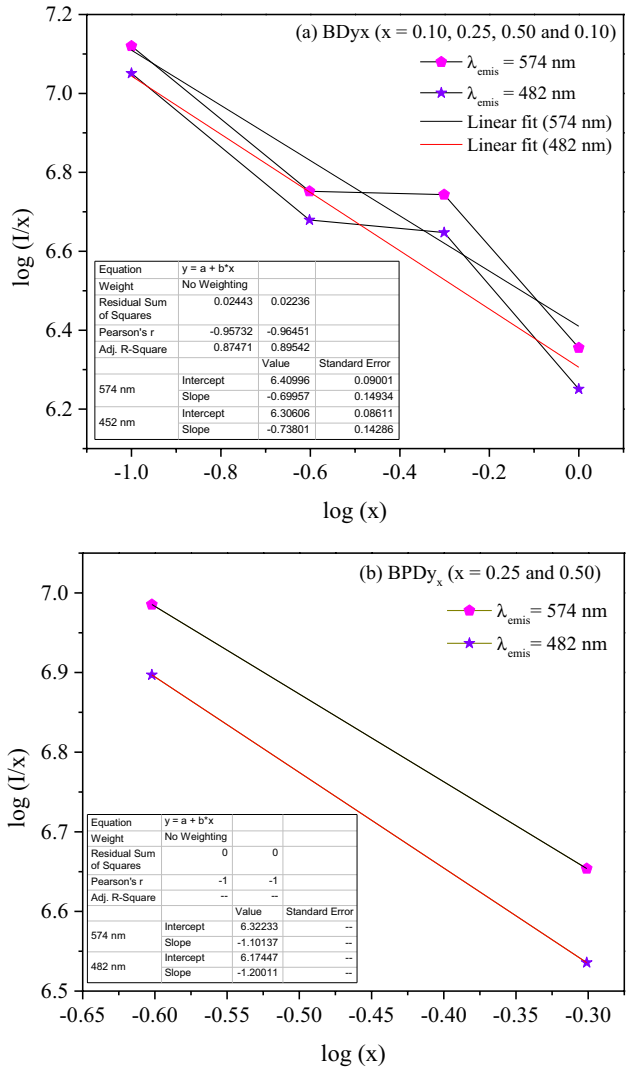

Fig. 10 (**a**, **b**) Linear fitting of log (*x*) vs. log (*I*/*x*) for borate (BDy_x, $x = 0.10$, 0.25, 0.50, and 1.00) and boro-phosphate ($BPDy_x$, $x = 0.25$ and 0.50) glasses

indicated by a ratio of Y/B increases. As a result, while the concentration of Dy^{3+} ions in the prepared glasses increases, it consequently increases the covalency of the Dy–O bond. The value of Y/B changes when Dy^{3+} is introduced in place of an element with a different valency ($Al^{3+/2+}$, Li^{3+}, Sr^{2+}, Ti^{2+}, and Zn^{2+}), and this change is proportional to variations in the concentration of Dy^{3+}. The local symmetry of Dy^{3+} will change with an increase in Dy^{3+} concentration because defects are produced in this circumstance. According to the gradual increase in Y/B ratios, the present glasses can produce blue or white light depending on the concentration of Dy^{3+} [47, 48].

The PL decay curves of BDy_x ($x = 0.25$ and 0.50) and $BPDy_x$ ($x = 0.25$ and 0.50) glasses are displayed in Fig. 11. For all the prepared glass networks, the decay rates of emission exhibit a non-exponential configuration. The Dy^{3+} non-exponential decay curves were fitted to the subsequent tri-exponential function:

$$I(t) = A_1 \exp\left(-\frac{t}{\tau_1}\right) + A_2 \exp\left(-\frac{t}{\tau_2}\right) + A_3 \exp\left(-\frac{t}{\tau_3}\right) \quad (12)$$

where, τ_1, τ_2, and τ_3 are the fluorescence lifetime components that undergo calculating the average lifespan, while A_1, A_2, and A_3 stand for the amplitudes of the corresponding decay components. The expression that follows can be used to determine the average lifespan for a non-exponential with three components [49].

$$\tau_{avg} = \frac{A_1\tau_1^2 + A_2\tau_2^2 + A_3\tau_3^2}{A_1\tau_1 + A_2\tau_2 + A_3\tau_3} \quad (13)$$

The Dy^{3+} ion concentration influences the $^4F_{9/2}$ fluorescence lifetime. For BDy_x glasses, the mean lifespan values decreased from 1.490 to 1.190 ms with an increase in Dy^{3+} dopant concentration; however, the value of 1.082 ms remained the same for $BPDy_x$ glasses. Effective lifetimes tend to be shortened as Dy^{3+} concentration rises; this is likely due to energy transfer within luminescence quenching centers, via the cross-relaxation (CR) process, and energy transfer from impurities [50]. In the present study, this behavior is explained by a substantial quenching as the dopant concentration increases and the distance between consecutive ions decreases. Therefore, there is a higher chance that the resonant interaction of energy within the Dy^{3+} ions will increase, leading to quicker fluorescence decay [51]. The non-radiative transmission of energy via cross-relaxation is schematically represented in Fig. 12. Three cross-relaxation channels could be discovered based on the energy resonance [2]. The excited Dy^{3+} ions relaxed from $^4F_{9/2}$ level to $^6F_{11/2}$ (CH-1), $^6F_{5/2}$ (CH-2), or $^6F_{3/2}$ (CH-3) level by transmitting its energy non-radiatively to another Dy^{3+} ions in $^6H_{15/2}$ level (ground state) and the energy acquired Dy^{3+} ions excite to $^6F_{3/2}$ (CH-1), $^6F_{9/2}$ (CH-2), or $^6F_{11/2}$ (CH-3)state. All the Dy^{3+} ions will relax to their ground state non-radiatively which results in the luminescence quenching.

The Inokuti-Hirayama model was used to evaluate the decay curve to explicate the energy migration between Dy^{3+}-Dy^{3+} ions [26].

$$I(t) = I_0 \exp\left[-\frac{t}{\tau} - Q\left(\frac{t}{\tau}\right)^{3/S}\right] \quad (14)$$

I_0 is the initial emission intensity; τ represents the intrinsic lifetime of donors, and Q is the energy transfer parameter, which is expressed as follows:

$$Q = \frac{4}{3}\pi\Gamma\left(1 - \frac{3}{S}\right)N_A R_c^3 \quad (15)$$

Table 4 Van Uitert parameter (θ) and Y/B ratio of borate (BDy_x, $x=0.10$, 0.25, 0.50, and 1.00) and boro-phosphate ($BPDy_x$, $x=0.25$ and 0.50) host network glasses

Glass	Dy^{3+} (wt%)	$\lambda_{em}=482$ nm		$\lambda_{em}=574$ nm		Y/B ratio
		$-\theta/3$	θ	$-\theta/3$	θ	
Borate host						
BDy0.10	0.10	0.738	2.241	0.699	2.099	1.233
BDy0.25	0.25					1.262
BDy0.50	0.50					1.288
BDy1.00	1.00					1.352
Boro-phosphate host						
BPDy0.25	0.25	1.200	3.600	1.101	3.303	1.218
BPDy0.50	0.50					1.298
Dy0.1 [54]	0.10					1.66
Dy0.5 [54]	0.50					1.67
Dy1.0 [54]	1.00					1.70
DFBP [53]	1.00					1.447
BPAbLiDy 1.0 [55]	1.00					0.945

where Γ is Euler's gamma function, and S is the multipolar interaction parameter. N_A represents Dy^{3+} concentration, and R_c denotes critical transfer distance. Figures 13 and 14 show the Inokuti-Hirayama fit for the decay profile of the BDy_x and $BPDy_x$ ($x=0.25$ and 0.50) glasses. The donor–acceptor ion interaction parameter (C_{DA}) and the shortest distance between the randomly distributed RE ions can be determined from the following equations [52]:

$$C_{DA} = \frac{R_c^S}{\tau} \tag{16}$$

$$D_{random} = 2\left(\frac{3}{4\pi N_T}\right)^{1/3} \tag{17}$$

The cross-relaxation between donor and acceptor could be the predominant reason for non-mono exponential behavior in all the samples. $D_{random} >> C_{DA}$ suggests the cross-relaxation and energy transfer probably occur among the Dy^{3+} clusters ions and not out of randomly distributed ions. Table 5 shows the lifetime value, energy transfer, and other related parameters derived from the PL Decay curve of BDy_x and $BPDy_x$ ($x=0.25$ and 0.50) glasses.

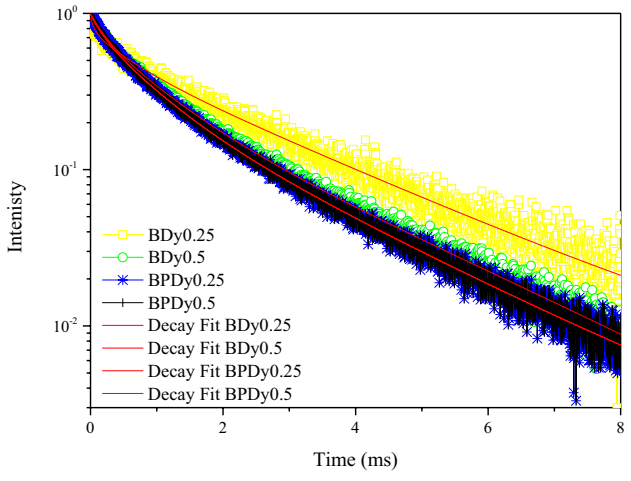

Fig. 11 Fluorescence decay profile of BDy_x and $BPDy_x$ glasses, where $x=0.25$ and 0.50 mol%

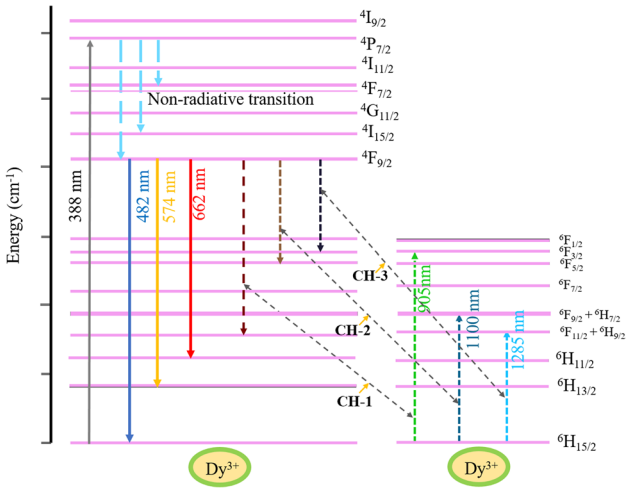

Fig. 12 Energy level structure of Dy^{3+} ion: cross-relaxation pathways through the energy resonance

3.7 CIE chromaticity coordinates

The color coordinates are one of the crucial components for assessing the effectiveness of the glasses' color rendering activity.

$$x = \frac{X}{X+Y+Z}, y = \frac{Y}{X+Y+Z} \text{ and } z = \frac{Z}{X+Y+Z} \quad (18)$$

where X, Y, and Z stand for the three tristimulus values and can be obtained by:

$$X = \int \bar{x}(\lambda)P(\lambda)d\lambda, Y = \int \bar{y}(\lambda)P(\lambda)d\lambda \text{ and } Z = \int \bar{z}(\lambda)P(\lambda)d\lambda \quad (19)$$

where $\bar{x}(\lambda), \bar{y}(\lambda)$, and $\bar{z}(\lambda)$ are color-matching functions, λ is the wavelength of the analogous monochromatic light, and $P(\lambda)$ is a spectral power distribution. Another significant factor for better understanding sources of light for LED applications is color purity or color saturation.

$$P_c = \frac{\sqrt{((x_s - x_i)^2 + (y_s - y_i)^2)}}{\sqrt{((x_d - x_i)^2 + (y_d - y_i)^2)}} \times 100\% \quad (20)$$

where (x,y), (x_i, y_i), and (x_d, y_d) represent the luminescent chromaticity coordinates, the standard white emission CIE coordinates (0.330, 0.330), and the dominant wavelength coordinates, respectively. The CIE chromaticity coordinates (x, y) of the present glasses with various concentrations of Dy^{3+} have been measured from the luminescence spectra and are discovered to (0.312, 0.314), (0.310, 0.313), (0.323, 0.335), and (0.328, 0.344) for BDy_x (x=0.10, 0.25, 0.50, and 1.00), whereas the values are (0.293, 0.293) for $BPDy_{0.25}$ and (0.317, 0.332) for $BPDy_{0.50}$ glass. The color purity (P_c) of conventional white light is 0%; the P_c of the BDy_x glasses was found to vary between 9.5 and 2.2%, whereas P_c of

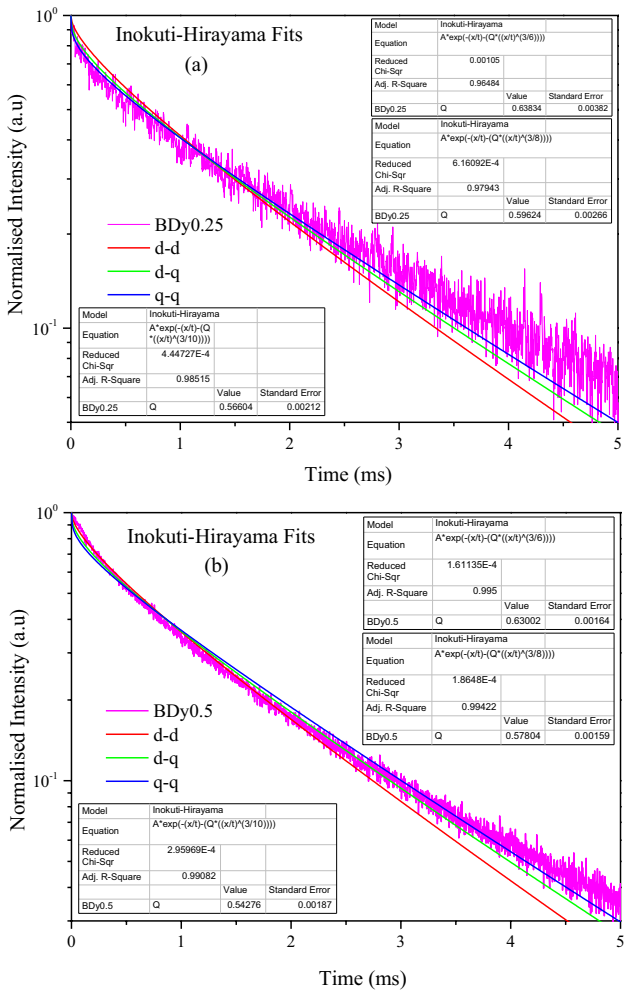

Fig. 13 Inokuti-Hirayama fit of borate host: (**a**) BDy0.25 and (**b**) BDy0.50 glasses

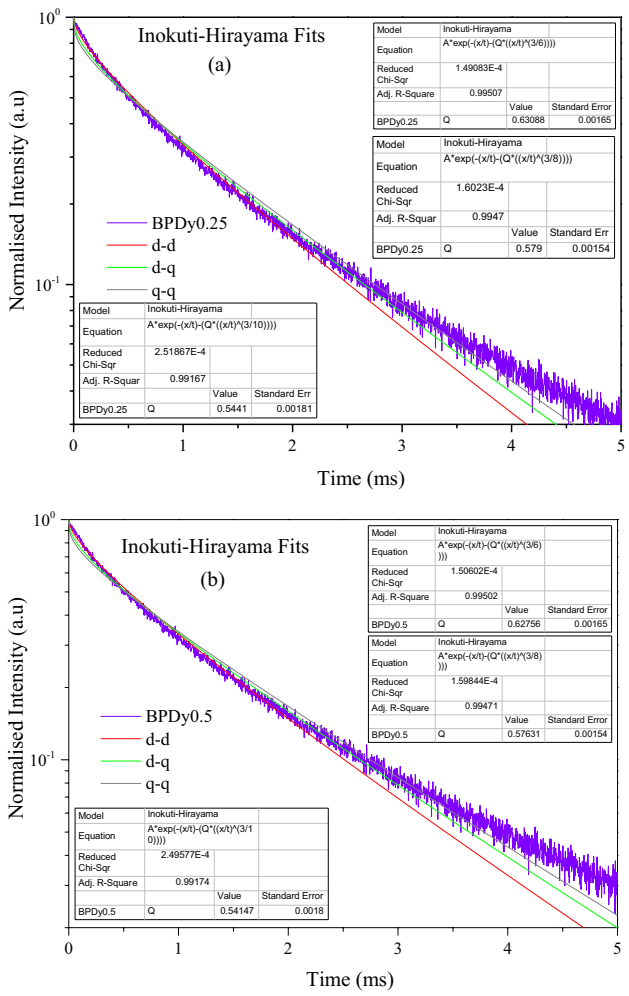

Fig. 14 Inokuti-Hirayama fit of boro-phosphate host: (**a**) BPDy0.25 and (**b**) BPDy0.50 glasses

Table 5 Experimental life time (T_{exp}), concentration of the acceptor (N_A), critical transfer distance (R_c), donor–acceptor ions interaction parameter (C_{DA}), and shortest distance between the randomly distributed RE ions (D_{random}) value of BDy_x and $BPDy_x$ ($x = 0.25$ and 0.50) glasses

Glass code	T_{exp} (ms)	N_A (ions/cm^3)	Q	R_c (Å)	C_{DA} (cm^6/s)	D_{random} (Å)
BDy0.25	1.49	1.112×10^{20}	0.638	9.181	4.02×10^{-40}	25.8
BDy0.5	1.19	2.206×10^{20}	0.63	7.276	1.25×10^{-40}	20.5
BPDy0.25	1.08	0.952×10^{20}	0.631	9.633	7.40×10^{-40}	27.2
BPDy0.5	1.08	1.887×10^{20}	0.627	7.669	1.88×10^{-40}	21.6
Dy 0.1 [54]	0.673	-	-	-	-	-
Dy 0.5 [54]	0.521	-	-	-	-	-
Dy 1.0 [54]	0.4207	-	-	-	-	-

$BPDy_x$ glasses varied between 17.5 and 5.5%. Furthermore, the P_c value of the glasses was found to increase as Dy concentrations increased.

Figure 15 depicts the distribution of chromaticity coordinates in the CIE 1931 chromaticity diagram. The chromaticity coordinates move to the yellow-white zone when Dy^{3+} concentration increases, indicating that warm white light is generated. Lower quantities of Dy^{3+} in a glass demonstrated that emission occurred in the blue-white region, as validated by their predominated wavelengths (λ_d) as well as the color purity (P_c). Correlated color temperature (CCT) is an essential technique for illuminant critical features. The point of white light area achieved for BDy0.5 may be also made to correspond with reference white light by adjusting the excitation wavelengths and calcination temperature. The CCT of prepared BDy_x and $BPDy_x$ glasses was computed using McCamy's relation from the chromaticity coordinates (x and y): $CCT = -437\ n^3 + 3601\ n^2 - 6861\ n + 5514.31$.

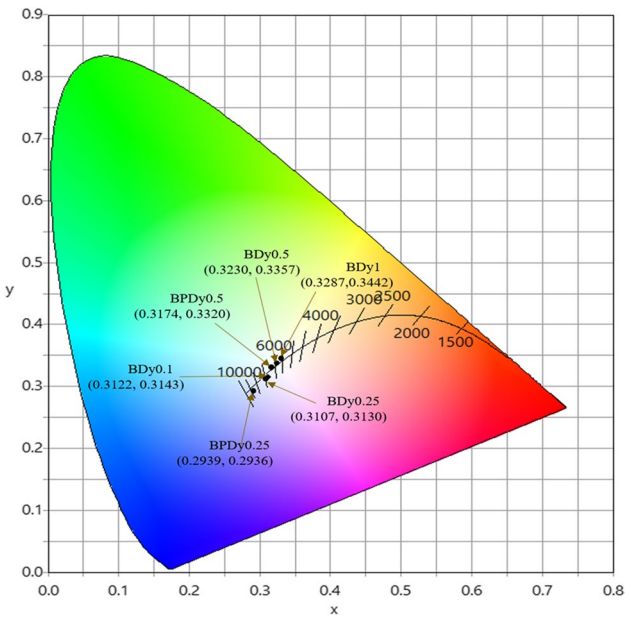

Fig. 15 CIE 1931 chromaticity coordinates of borate (BDy_x, $x = 0.10$, 0.25, 0.50, and 1.00) and boro-phosphate ($BPDy_x$, $x = 0.25$ and 0.50) glasses

Where $n = (x - 0.3320)/(y - 0.1858)$; x and y are the CIE chromaticity coordinates. Natural white light can be classified into three broad zones based on CCT values: cool white (> 5000 K), pure white (3700–5000 K), and warm white (< 3700 K). A CCT value greater than 5000 K suggests cool white light from the glasses. Table 6 shows that the CCT values of borate host glasses range from 5664 to 6769 K, and those of boro-phosphate host glasses vary from 6237 to 8432 K. CCT values of more than 5000 K were found in Dy^{3+}-doped borate and boro-phosphate glass networks; when compared with recent literature, the prepared glasses showed a cool white light emission.

4 Conclusions

Dy^{3+} ions doped in two different hosts; borate (BDy_x) and boro-phosphate ($BPDy_x$) glasses were prepared by the melt-quenching technique. The vibrational analysis of glasses confirmed that an increase in the concentration of Dy^{3+} ions increases the conversion of BO_3 units into BO_4 tetrahedral units, which leads to a decrease in the maximum phonon energy of the glass system and an increase in the intensity of luminescence. The BDy0.5 and BDy1.0 glasses exhibited a lower Urbach energy, indicating a

Table 6 CIE chromaticity coordinates, color coordinates, CCT, and dominant wavelength of prepared BDy_x ($x = 0.10$, 0.25, 0.50, and 1.00) and $BPDy_x$ ($x = 0.25$ and 0.50) glasses

Glasses	x	y	CCT (K)	λ_d (nm)	P_c (%)
BDy0.10	0.3122	0.3143	6661	478.7	8.9
BDy0.25	0.3107	0.3130	6769	478.8	9.5
BDy0.50	0.323	0.3357	5942	494.7	3.3
BDy1.00	0.3287	0.3442	5664	526.7	2.2
BPDy0.25	0.2939	0.2936	8432	476.8	17.5
BPDy0.50	0.3174	0.332	6237	490.7	5.5
Dy 0.1 [54]	0.376	0.402	4247	-	-
Dy 0.5 [54]	0.374	0.397	4298	-	-
Dy 1.0 [54]	0.376	0.399	4407	-	-
DFBP [53]	0.383	0.419	4203	571.6	47.1

lesser phonon state disruption that leads to excellent emission characteristics. The resonance processes in the borate host matrix cause the BDy0.5 glass to react more prominently in non-linear optical characteristics. The PL spectra showed that a dipole–dipole interaction influences the concentration quenching over 0.5 wt% and 0.25 wt% of Dy^{3+} dopant in a borate and boro-phosphate glass network, respectively. The Inokuti-Hirayama fit also confirms the dominance of dipole–dipole interaction energy transfer between acceptor–donor ions. With increasing Dy^{3+} concentration, the bluish-white color of the BDy_x and $BPDy_x$ glasses shifted to yellowish-white with extreme color purity. Among all the prepared glasses, BDy0.5 had a CCT value of 5942 K and color coordinates of (0.323, 0.335), indicating it is a promising cool-white light emitting glass for optical lighting applications.

Acknowledgements We thank BRNS for the Project, entitled "Synthesis of novel Ln incorporated nonsilicate glass ceramics as radiation shielding materials," No. 59/14/07/2020-BRNS/10096.

Data availability All data generated or analyzed during this study are included in this published article.

Declarations

Conflict of interest The authors declare no competing interests.

References

1. J. Gangareddy, H. Syed, S. Chakraborty, P. Sen, M. Ghosh, K.K. Dey, K. Bhattacharyya, K. Annapurna, V.R. Soma, A.R. Allu, Tunable, efficient, ultrafast broadband nonlinear optical properties of TiO2-loaded complex phosphate glasses. Mat. Res. Bull. **167**, 112141 (2023). https://doi.org/10.1016/j.materresbull.2023.112414
2. S. Kaur, D. Arora, S. Kumar, G. Singh, S. Mohan, P. Kumar, P. Kriti, D.P. Singh. Kaur, Blue-yellow emission adjustability with aluminium incorporation for cool to warm white light generation in dysprosium doped borate glasses. J Lumin **202**, 168–175 (2018). https://doi.org/10.1016/j.jlumin.2018.05.034
3. G.A. Kumar, A. Martinez, E. Mejia, J.G. Eden, Fluorescence and upconversion spectral studies of Ho3+ in alkali bismuth gallate glasses. J. Alloys and Comp. **365**, 117–120 (2004). https://doi.org/10.1016/S0925-8388(03)00650-9
4. L. Shamshad, G. Rooh, K. Kirdsiri, N. Srisittipokakun, B. Damdee, H.J. Kim, J. Kaewkhao, Photoluminescence and white light generation behavior of lithium gadolinium silicoborate glasses. J. Alloy. Compd. **695**, 2347–2355 (2017). https://doi.org/10.1016/j.jallcom.2016.11.105
5. J. Kaewkhao, N. Wantana, S. Kaewjaeng, S. Kothan, H.J. Kim, Luminescence characteristics of Dy3+ doped Gd2O3-CaO-SiO2-B2O3 scintillating glasses. J. Rare Earth **34**(6), 583–589 (2016). https://doi.org/10.1016/S1002-0721(16)60065-0
6. L.H. Jiang, Y.L. Zhang, C.Y. Li, J.Q. Hao, Q. Su, Thermoluminescence studies of LiSrBO3: RE3+ (RE= Dy, Tb, Tm, and Ce). Appl. Radiat. Isot. **68**(1), 196–200 (2010). https://doi.org/10.1016/j.apradiso.2009.10.001
7. K. Biswas, A.D. Sontakke, K. Annapurna, Effect of TiO2 on thermal, structural and third-order nonlinear optical properties of Ca – La – B – O glass system. J Alloy Compd **489**, 493–498 (2010)
8. Camila DS. Bordon, Evellyn S. Magalhaes, Davinson M. da Silva, Luciana RP. Kassab, Cid B. de Araújo, Influence of Al2O3 on the photoluminescence and optical gain performance of Nd3+ doped germanate and tellurite glasses. Opt Mat **109**, 110342 (2020). https://doi.org/10.1016/j.optmat.2020.110342
9. B. Hari Babu, V.V. Ravi Kanth Kumar, Warm white light generation in γ-irradiated Dy3+, Eu3+ codoped sodium aluminoborate glasses. J Lumin. **169**, 16–23 (2016). https://doi.org/10.1016/j.jlumin.2015.08.058
10. P.P. Pawar, S.R. Munishwar, R.S. Gedam, Intense white light luminescent Dy3+ doped lithium borate glasses for W-LED: A correlation between physical, thermal, structural and optical properties. J. Sol. State. Sci. **64**, 41–50 (2017). https://doi.org/10.1016/j.solidstatesciences.2016.12.009
11. D. Singh, K. Singh, B.S. Bajwa, G.S. Mudahar, D.P. Singh, Manupriya Manupriya, M. Arora, V.K. Dangwal, Optical and structural properties of Li2O–Al2O3–B2O3 glasses before and after γ-irradiation effects. J. Appl. Phys. **104**, 10 (2008). https://doi.org/10.1063/1.3003070
12 S. Kaur, Amit K. Vishwakarma, Aman Prasad NishaDeopa, M. Jayasimhadri, Spectroscopic studies of Dy3+ doped borate glasses for cool white light generation. Mat. Res. Bull. **104**, 77–82 (2018). https://doi.org/10.1016/j.materresbull.2018.04.002
13. F.H. ElBatal, S. Ibrahim, A.M. Abdelghany, Optical and FTIR spectra of NdF3-doped borophosphate glasses and effect of gamma irradiation. J. Mol. Struct. **1030**, 107–112 (2012). https://doi.org/10.1016/j.molstruc.2012.02.049
14. Sd. Zulfiqar Ali Ahamed, C. Madhukar Reddy, B. Deva Prasad Raju, Structural, thermal, and optical investigations of Dy3+ ions doped lead containing lithium fluoroborate glasses for simulation of white light, Opt. Mat. **35**, 1385 – 1394 (2013) https://doi.org/10.1016/j.optmat.2013.02.006
15. Hideharu Ushida, Yasuhiko Iwadate, Takeo Hattori, Shin Nishiyama, Kazuko Fukushima, Yasuhisa Ikeda, Makoto Yamaguchi et al., Network structure of B2O3–PbO and B2O3–PbO–PbBr 2 glasses analyzed by pulsed neutron diffraction and Raman spectroscopy. J. Alloys Compd. **377**(1–2), 167–173 (2004). https://doi.org/10.1016/j.jallcom.2003.12.038
16. S.R. Rejisha, P.S. Anjana, N. Gopakumar, N. Santha, Synthesis and characterization of strontium and barium bismuth borate glass-ceramics. J. Non-Cryst. Sol. **388**, 68–74 (2014). https://doi.org/10.1016/j.jnoncrysol.2014.01.037
17. B.N. Meera, J. Ramakrishna, Raman spectral studies of borate glasses. J. Non-Cryst. Solids **159**(1–2), 1–21 (1993). https://doi.org/10.1016/0022-3093(93)91277-A
18. C.N. Santos, D.D.S. Meneses, P. Echegut, D.R. Neuvile, A.C. Hernandes, A. Lbanez, Appl. Phys. Lett. **94**, 15190–151903 (2009)
19. R.C. Lucacel, V. Carmen Marcus, I. Timar, Ardelean, FT-IR and FT-Raman spectroscopic studies on B2O3-PbO-Ag2O glasses doped with manganese ions. J. Sol. Stat. Sci. **9**, 850–854 (2007). https://doi.org/10.1016/j.solidstatesciences.2007.07.006
20 B. Deva Prasad Raju, C. Madhukarreddy, Structural and optical investigations of Eu3+ ions in lead-containing alkali fluoroborate glasses Opt. Mat. **34**, 1251–1260 (2012). https://doi.org/10.1016/j.optmat.2012.01.027
21. M. Dhavamurthy, P. Vinothkumar, Manoj Mohapatra, Antony Suresh, Priya Murugasen, Effects of Ce^{3+}/Dy^{3+} and Ce^{3+}/Sm^{3+} co-doping as a luminescent modifier in alumina-borophosphate glasses for w-LED applications, Spectchim. Act. Part A: Mol. Biomol. Spect. **266**, 120448 (2022). https://doi.org/10.1016/j.saa.2021.120448

22. M. Anastasopoulou, K.C. Vasilopoulos, D. Anagnostopoulos, I. Koutselas, D.K. Papayannis, M.A. Karakassides, Structural and theoretical study of strontium borophosphate glasses using Raman spectroscopy and ab initio molecular orbital method. J. Phys. Chem. B **121**, 4610–4619 (2017). https://doi.org/10.1021/acs.jpcb.7b01563
23 P. Ramakrishna, P. Sitakanta Panda, R.K. Padhi. Vinodkumar, B. Hrudananda Jena, S. Panigrahi, Structural and optical properties of cerium and dysprosium coactivated borophosphate glasses for cool white light application. J Non-Cryst Sol **566**, 120883 (2021). https://doi.org/10.1016/j.jnoncrysol.2021.120883
24. D. Carta, D. Qiu, Paul Guerry, Ifty Ahmed, Ensanya A. Abou, Jonathan C. Neel, Mark E. Knowles, Robert J. Smith, Newport, The effect of composition on the structure of sodium borophosphate glasses. J. Non-Cryst. Sol. **354**, 3671–3677 (2008). https://doi.org/10.1016/j.jnoncrysol.2008.04.009
25 E. Cavalli, Optical spectroscopy of Dy3+ in crystalline hosts: general aspects, personal considerations and some news. J Opt Mat X **1**, 100014 (2019). https://doi.org/10.1016/j.omx.2019.100014
26 M. Priya, M. Dhavamurthy, A. Antony Suresh, M. MonojMohapatra, Luminescence and spectroscopic studies on Eu3+- doped borate and boro-phosphate glasses for solid-state optical devices. J. Opt. Mat. **142**, 114007 (2023). https://doi.org/10.1016/j.optmat.2023.114007
27 S. Ibrahim, Manal Abdel-Baki, Fouad El-Diasty, Zinc borophosphate glasses for infrared-based optical applications. Opt. Eng. **51**(9), 093401–093401 (2012). https://doi.org/10.1117/1.OE.51.9.093401
28. S.H. Wemple, Optical oscillator strengths and excitation energies in solids, liquids, and molecules. J. Chem. Phys. **67**(5), 2151–2168 (1977). https://doi.org/10.1063/1.435102
29. O. Fanderlik, *properties of glass* (Elsevier Publishing Company, Amesterdam, 1983)
30. H. Scholze, *Glass nature, structure and properties* (Springer, Berlin, 1990)
31 F.M. Ezz El-Din, N.A. El-Alaily, H.A. El-Batal, Chem. **163**, 267–275 (1992). https://doi.org/10.1007/BF02034800
32. J. Dahiya, A. Hooda, Ashish Agarwal, Satish Khasa, Effect of dysprocium and samarium RE ion co-doping on photoluminescence behavior of novel alkali fluride bismuth borate glasses: a white LED materials. Opt. Mat. **134**, 113162 (2022). https://doi.org/10.1016/j.optmat.2022.113162
33. G. Lakshminarayana, A.N. Meza-Rocha, O. Sariano-Romero, E.F. Huerta, U. Caldino, A. Lira, Dong-Eun Lee, Jonghun Yoon, Taejoon Park, Pr3+-doped B2O3-Bi2O3-ZnO-NaF glasses comprising alkali mixed alkali oxides for potential warm white light generation, blue laser, and E-+S-+C-optical bands amplification applications. J. Mater. Res. Technol. **13**, 2501–2526 (2021). https://doi.org/10.1016/j.jmrt.2021.06.037
34. A.M. Ibrahim, A.H. Hammad, A.M. Abdelghany, G.O. Rabie, Mixed alkali effect and samarium ions effectiveness on the structural, optical and non-linear optical properties of borate glass. J. Non-Cryst. Solids **495**, 67–74 (2018). https://doi.org/10.1016/j.jnoncrysol.2018.05.015
35. J.J. Wynne, Optical third-order mixing in GaAs, Ge, Si, and InAs. Phys. Rev. **178**, 1295–1303 (1969). https://doi.org/10.1103/PhysRev.178.1295
36. K. Terashima, Sae-Hoon Kin, Toshinobu Yoko, Nonlinear optical properties of B2O3-based glasses: M2O–B2O3 (M = Li, Na, K, Rb, Cs, and Ag) binary borate glasses. J. Am. Ceram. Soc. **78**(6), 1601–1605 (1995). https://doi.org/10.1111/j.1151-2916.1995.tb08857.x
37. K. Terashima, Suguru Tamura, Sea-Hoon Kim, Toshinobu Yoko, Structure and nonlinear optical properties of lanthanide borate glasses. J. Am. Ceram. Soc. **80**(11), 2903–2909 (1997). https://doi.org/10.1111/j.1151-2916.1997.tb03210.x
38. H. Nasu, J. Mastsuoka, O. Sugimoto, M. Kida, K. Kamiya, Non-resonant type third-order optical nonlinearity of rare earth oxides – containing GeO2 glasses. J. Ceram. Soc. Jpn. **101**, 43–47 (1993). https://doi.org/10.2109/jcersj.101.43
39. D. Gao, Yunci Li, Lihong Cheng, Shengyi Liu, Sai Xu, Xiangping Li, Jinsu Zhang, Xizhen Zhang, Yongze Cao, Yichao Wang, Xin Wang, Yuhang Zhang, Xuezhu Sha, Li Wang, Baojiu Chen, Concentration effects of fluorescence quenching and optical transtition properties of Dy3+ doped NaYF4 phosphor. J. Alloys and Comp. **895**, 162616 (2022). https://doi.org/10.1016/j.jallcom.2021.162616
40. L. Chih-Hao, Lay-Gaik. Teoh, Kuan Ting Liu, Yee-Shin. Chang, Near white light, emission of BaY2ZnO5 doped with Dy3+ ions. J. Alloys and Comp. **517**, 9–13 (2012). https://doi.org/10.1016/j.jallcom.2011.11.088
41. X. Zhang, Fangui Meng, Wnelan Li al, Sun II Kim, Young Moon Yu, Hyo Jin Seo, Investigation of energy transfer and concentration quenching ofDy3+ luminescence in Gd(BO2)3 by means of fluorescence dynamics. J. Alloys and Comp. **578**, 72–76 (2013). https://doi.org/10.1016/j.jallcom.2013.05.012
42. X. Li, P. Li, Z. Wang, S. Liu, Q. Bao, X. Meng, K. Qiu, Y. Li, Z. Li, Z. Yang, Color-tunable luminescence properties of Bi^{3+} in $Ca_5(BO_3)_3F$ via changing site occupation and energy transfer. Chem. Mater. **29**(20), 8792–8803 (2017). https://doi.org/10.1021/acs.chemmater.7b03151
43. Z. Zhu, C. Tao, Z. Wang, Z. Yang, P. Li, Luminescence and energy transfer of warm white-emitting phosphor Mg2Y2Al2Si2O12 Dy3+, Eu3+ for white LEDs. RSC Ad **11**, 32707–32716 (2021). https://doi.org/10.1039/d1ra06215h
44. L.G. Van Uitert, Characterization of energy transfer interaction between rare earth ions. J. Elect. Chem. Soc. **114**, 1048 (1967). https://doi.org/10.1149/1.2424184
45. K. Saidi, M. Dammak, Crystal structure, optical spectroscopy and energy transfer properties in NaZnPO4:Ce3+, Tb3+ phosphors for UV-based LEDs. RSC Adv. **10**(37), 21867–21875 (2021). https://doi.org/10.1039/d0ra04163g
46. S. Arunkumar, G. Venkataiah, K. Marimuthu, Spectroscopic and energy transfer behaviour of Dy3+ ions in B2O3-Teo-PbO-PbF2-BiO3-CdO glasses for laser and WLED applications, Spectrochem Acta Part A Mol. Biomol. Spectrosc. **16**, 1684–1697 (2015). https://doi.org/10.1016/j.saa.2014.10.067
47. Q. Su, Zhiwu Pei, Lisheng Chi, Hongjie Zhang, Zhongyi Zhang, Feng Zou, The yellow-to-blue intensity ratio (Y/B) of Dy3+ emission. J. Alloys and Comp. **192**, 25–27 (1993). https://doi.org/10.1016/0925-8388(93)90174-L
48. K. Linganna, Ch Srinivasa Rao, C.K. Jayasankar, Optical properties and generation of white light in Dy3+-doped lead phosphate glasses. J. Quant. Spectrosc. Radiat. Transf. **118**, 40–48 (2013). https://doi.org/10.1016/j.jqsrt.2012.12.002
49. B. Grobelna, A. Synak, P. Bojarski, K. Szczodrowski, B. Kuklinski, S. Raut, I. Gryczynski, Synthesis and luminescence of Dy3+ ions in silica xerogels doped with Ln2-xDyx(WO4)3. J. Opt. Mat. **35**, 456–461 (2013). https://doi.org/10.1016/j.optmat.2012.09.040
50. P. Haritha, I. R Martin, C.S. Dwaraka Viswanath, N. Vijaya, K. Venkata Krishnaiah, C. K. Haranath, V. Lavin, V. Venkataramu, J. Opt. Mater. **70**, 16 – 24 (2017). https://doi.org/10.1016/j.opmat.2017.05.002
51. S. Chemingui, M. Ferhi, K. Horchani-Naifer, M. Ferid, Synthesis and luminescence characteristics of Dy3+ doped KLa(PO3)4. J. Lumin. **166**, 82–87 (2015). https://doi.org/10.1016/j.jlumin.2015.05.018

52. M.E. Alvarez-Ramos, Luminescence and study of channels for cross-relaxation dependent on the concentration of Sm3+ under simultaneous UV-IR excitation in tellurite-germanate glasses. J. Alloys Compd. **854**, 157076 (2021). https://doi.org/10.1016/j.jallcom.2020.157076
53. M. Priya, P. Dhavamurthy, A. Antony Suresh, Manoj Mohapatra, Structural, optical, and thermoluminescence characterizations of 1 mol% Dy3+ ion-activated fluro boro-phosphate glass for photonic devices. Spectchim Act Part A: Mol Biomol Spect **308**, 123757 (2024)
54 M. Monisha, G. NirmalMazumder, Soumen Mandal Lakshminarayana, Sudha D. Kamath, Energy transfer and luminescence study of Dy3+ doped zinc-aluminoborosilicate glasses for white light emission. Ceram. Int. **47**(1), 598–610 (2021). https://doi.org/10.1016/j.ceramint.2020.08.167
55. P. Arun. Joseph, K. Maheshvaran. Jeganatha, I. Arul Rayappan, Structural and optical studies on Dy3+ ions doped alkali lead borophosphate glasses for white light applications. J Non-Cryst Solids **557**, 120652 (2021)